ELSEVIER

Journal of Alloys and Compounds 271–273 (1998) 322–326

Journal of ALLOYS AND COMPOUNDS

Fission mechanisms in the carbon-induced fission of uranium

A. Yokoyama*, H. Baba, N. Takahashi, T. Saito

Department of Chemistry, Graduate School of Science, Osaka University, 1-1 Machikaneyama, Toyonaka, Osaka 560, Japan

Abstract

The conventional radiochemical technique was applied to the ^{12}C-induced fission of ^{238}U at incident energies below and above the borderline for the appearance of fast fission. It supplies information on the charge dispersion and distribution of fission products in addition to the mass distribution for isolation of fast fission from ordinary fusion fission. The resulted width of charge dispersion was independent of *A* except for the case of the 140 MeV incident energy, where the widths at far-asymmetric mass region were definitely large compared to the normal value. On the other hand, the observed variances of mass distribution change around the threshold energy for fast fission more drastically than prediction by the model assuming that they are controlled by the stiffness coefficient and the temperature. We conclude that both results suggest the appearance of far-asymmetric mass distribution associated with the set-in of fast fission. © 1998 Elsevier Science S.A.

Keywords: Heavy-ion fission; Uranium-238; Carbon-12; Charge dispersion; Mass distribution; Fast fission

1. Introduction

The effect of the angular momentum on the fission phenomenon appears as a decrease of the fission barrier [1–4]. The fission barrier finally vanishes when the angular momentum introduced to the compound nucleus exceeds a critical value ℓ_{B_f}. The fission with no fission barrier is called fast fission. Though the definition of fast fission is thus quite clear, the mechanism of formation of the system undertaking fast fission is not quite distinguished from deep inelastic scattering, quasi-fission, etc. The characteristics of fast fission are not very well known either in spite of several experimental and theoretical works [5–17].

Zheng et al. [12] also found that the difference in the total kinetic energy was too small to detect between fusion fission and fast fission. On the other hand, they observed substantial increase both in the widths of mass and kinetic energy distributions for fast fission.

No matter which mechanism is controlling fast fission, experiments tell us it is difficult to distinguish fast fission from normal fusion fission in terms of the product angular distribution, total kinetic energy or the mass asymmetric degree of freedom. Instead, widths of the mass and kinetic energy distributions are reported to be substantially large for fast fission compared to those of compound fission. The product charge distribution is also shown to be different between the two mechanisms.

The above consequences suggest the fast fission characteristics may be prominently observable in the form of broadening of the distribution width of various fission observables. On the other hand, it has been shown that counter experiments hardly succeeded in distinguishing fast fission phenomena from those of ordinary fusion fission. This is probably a consequence of smearing out of any fine structure in the distribution of fission observables due to finite mass and/or energy resolution.

The conventional radiochemical technique which is able to strictly specify *A* and *Z* of the product nuclei is expected to supply sufficient information to isolate fast fission from ordinary fusion fission and subsequently to shed light on the mechanism of fast fission.

The present purpose is thus to radiochemically investigate the characteristics of the ^{12}C-induced fission of ^{238}U at incident energies below and above the borderline for the appearance of fast fission. Any notable difference in the feature between them, if any, should demonstrate the fast fission characteristics.

2. Experimental

^{238}U targets were prepared by electrodeposition of UO_2 on Al backing foils. Details of the procedure are described

*Corresponding author. Tel.: +81-6-850-5417; fax: +81-6-850-5418; e-mail: yokoyama@chem.sci.osaka-u.ac.jp

PII: S0925-8388(98)00080-2

elsewhere [18]. The target assembly consisting of thus prepared ^{238}U target of about 1 mg/cm^2 in thickness and Al catcher foils to retain all fission product nuclei was irradiated with ^{12}C beams in a pneumatic irradiation facility installed in the AVF cyclotron at Research Center for Nuclear Physics, Osaka University.

^{238}U was irradiated with 110, 130, and 140 MeV ^{12}C for three hours and the irradiated target was subjected to off-line Ge γ-ray spectrometry. Thirty-minute irradiation was undertaken as well in order to determine the yields of short-lived activities. Further, iodine and rare earths were chemically separated as described elsewhere [19] in separate runs before Ge γ-ray measurement. Chemical yields were determined by comparing the yields of common nuclides between the destructive and non-destructive samples.

Obtained series of time-sequential γ-ray spectra were analyzed by BOB code [20], [21] to construct decay curves for individual yields of the relevant photopeaks at the end of bombardment (EOB). The energy and the half-life of the relevant γ-ray let us identify the nuclide to which the γ-ray belongs, and the obtained EOB value, corrected for the ingrowth during irradiation [22], is converted to the formation cross section. Gamma-ray emission probabilities and half-lives used to deduce cross section values were taken from [23].

3. Results and discussion

From the results, three or more isobaric yield data sets were obtained for several mass chains, from which we constructed charge dispersion curves by the least squares fit to the Gaussian distribution. Determined dispersion widths are plotted versus fragment mass A in Fig. 1. From the figure, we can draw the following conclusions; i) the width is independent of A except for the far-asymmetric mass division in the case of the 140 MeV incident energy and the constant width agreed with dispersion widths observed among various types of energetic fissions within the experimental error [19], ii) the charge dispersion in the mass chains $A=132$ and 134 reveals complex features indicating coexistence of complete and incomplete fusion fission as mentioned by Lee et al. [24], and iii) the widths at far-asymmetric mass region were definitely large for 140 MeV beam compared to the normal value.

The broadening of charge dispersion width in far-asymmetric mass region is expected to represent the effect of fast fission since it sets in above 110 MeV. That is, the products of fast fission may locate in the far asymmetric mass region only.

Results of the fission fragment angular correlation measurement [19] tell us the incomplete fusion fission takes place by fusion of ^{4}He with the incident velocity produced due to break-up of the ^{12}C projectiles. With this knowledge, we determined apparent most probable charges Z_p for mass chains in which two or more isobaric yields were given. The obtained Z_p values are shown in Fig. 2. The Z_p values are found to clearly follow a linear relationship (solid lines) with A in all the cases except for the double-magic mass region. In the top of Fig. 2, the

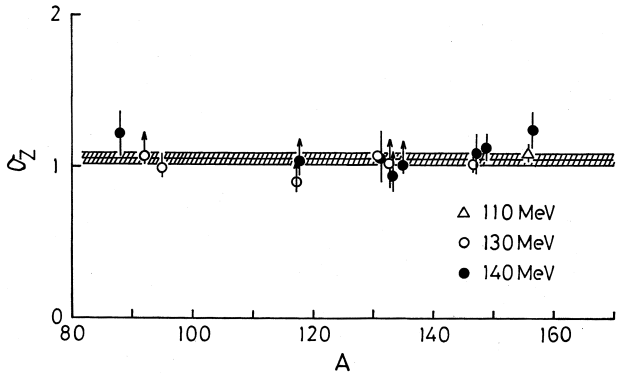

Fig. 1. Obtained width parameters plotted versus mass number A. The horizontal line with hatched band gives the weighted mean of the resulting widths except for the two outermost values at 140 MeV, namely, $<\sigma>=1.05\pm0.04$ charge unit.

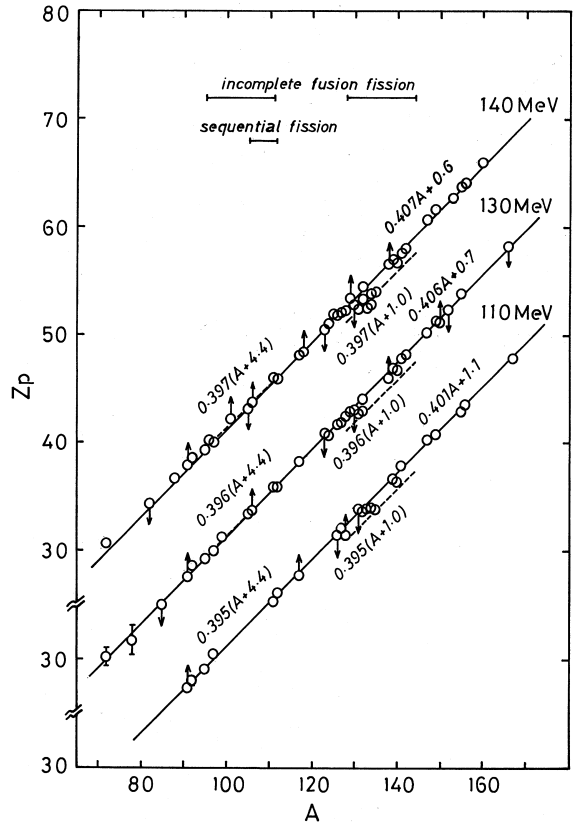

Fig. 2. Determined most probable charges plotted versus mass number. Solid lines represent the charge distribution of complete fusion/fast fission while dashed lines give that of incomplete fusion fission. Horizontal segments of lines indicate the mass regions where the incomplete fusion fission and sequential fission give substantial influence to the mass distribution in the case of the 240 MeV incident energy [24].

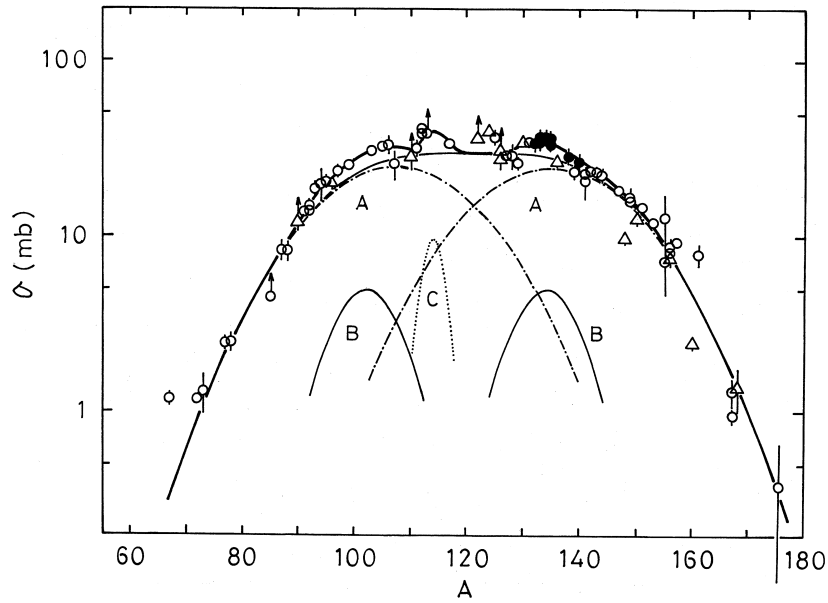

Fig. 3. Mass yield distribution for the 110 MeV ^{12}C beam. Circles represent the total chain yields determined with cumulative yields and triangles designate those obtained from independent yields. Solid marks are the chain yields evaluated by means of the duplicated charge distributions for complete and incomplete fusion fissions. The complete fusion fission component was fitted to a pair of Gaussian distributions represented with chain curves, while a pair of solid Gaussian curves give the incomplete fusion fission. A dotted curve corresponds to the sequential fission by Lee et al. [24]

regions where incomplete fusion fission and sequential fission give substantial influence are indicated with horizontal segments of line for the ^{238}U fission with 240 MeV carbon beam [24].

The charge distribution in the light-ion-induced fission can be systematically treated [25–27] as

$$Z_p = \frac{Z_c}{A_c - \nu_{pre}}\{A + \nu_{post}(A) \pm \Delta(A)\}, \quad (1)$$

where A_c and Z_c are the mass and charge of the compound nucleus, ν_{pre} and ν_{post} give the numbers of pre- and post-scission neutrons, and Δ is the charge polarization. Here, ν_{pre} is found to linearly depend on the excitation energy E_x;

$$\nu_{pre} = \frac{E_x}{\alpha} + \nu_0. \quad (2)$$

Then, we assumed the following values; $\alpha = 7.5$ MeV,

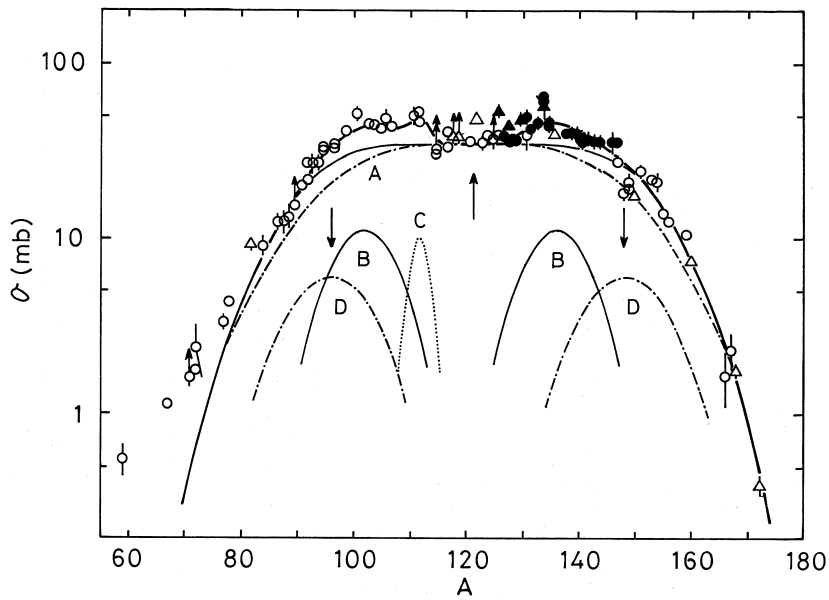

Fig. 4. Mass-yield distribution for the 130 MeV ^{12}C beam. The mass distribution depicted with a solid trapezoidal curve is considered to consist of complete fusion fission and fast fission which is decomposed into complete fusion (a trapezoidal chain curve) and incomplete fusion (a pair of Gaussian chain curves) fissions. The rest are the same as Fig. 3.

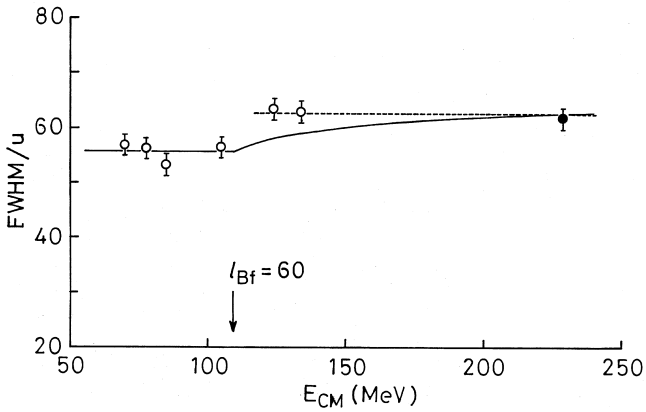

Fig. 5. FWHM of the mass-yield distribution of the complete-fusion/fast fission component as a function of the center-of-mass energy. The solid curve represents the energy dependence of FWHM when it is analyzed as Ref. [13].

$\nu_0 = 18.5 - Z_c^2/(2A_c)$, $\nu_{post} = 2.7$, and $\Delta = 1.7$ within the allowance range [25–27] for respective quantities. The resulting charge distribution of the incomplete fusion fission is indicated in Fig. 2 with dashed lines for each incident energy. One may recognize that the most probable charges in the light-fragment mass region of the incomplete fusion fission coincide with those of the complete fusion fission for all three cases. This makes the evaluation of the total chain yields quite easy in this region.

The mass-yield distribution for 110 MeV ^{12}C is shown in Fig. 3 in which complete fusion fission (A), incomplete fusion fission (B), and the so-called ''sequential fission (C)'' are extracted. Solid marks represent the sum of the total chain yields of complete and incomplete fusion fissions evaluated by applying two different charge distributions. The complete fusion fission distribution was determined by fitting the outskirts of the whole mass distribution to a pair of the identical Gaussian curves (chain lines) [19]. The surplus portions were then attributed to incomplete fusion and sequential fissions.

Fig. 4 represents the mass distribution for the 130 MeV ^{12}C beam deduced by a like procedure as in the case of Fig. 3. The gross distribution (thick full line) was decomposed into three components, complete-fusion fission plus fast fission (trapezoidal thin full line), incomplete-fusion fission (B), and sequential fission (C).

Since the maximum angular momentum brought in by the 110 MeV ^{12}C is close to $\ell_{B_f} = 60\ \hbar$, the fusion fission mass distribution for 130 or 140 MeV fission will be well approximated with that for 110 MeV when the height is slightly adjusted as depicted with a chain line (A) in Fig. 3 or Fig. 4. Hence, the difference (D) between the trapezoidal distribution and A-component is expected to give the fast fission mass distribution. The resulting fast fission mass distribution is consistent with the result obtained for the charge dispersion width (Fig. 1).

The widths of the obtained mass distributions are plotted versus center-of-mass energy E_{CM} in Fig. 5. The widths obtained at lower energies [19] are also added in the figure. The solid circle at 228 MeV is the re-evaluated width for the 240 MeV ^{12}C data [24] using a trapezoidal distribution which turns out to reproduce the observed yield data much better than the single Gaussian curve for fusion-plus-fast fission component as depicted in Fig. 6.

Now, let us assume the FWHM of the mass distributions of either fusion fission or fast fission is constant with respect to the incident energy and angular momentum. Then the total variance σ^2 is expressed in terms of the variances σ_1^2 and σ_2^2 of fusion fission and fast fission, respectively, as [13]

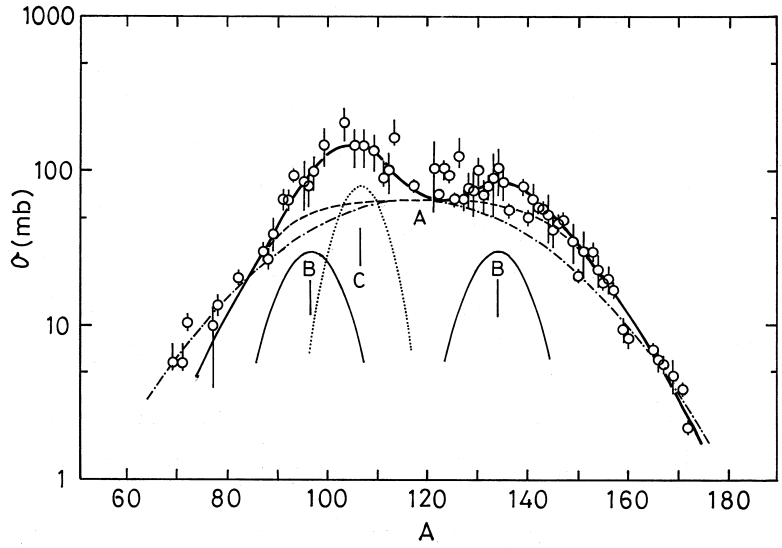

Fig. 6. The mass-yield distribution for the 240 MeV ^{12}C beam [24] in which a trapezoidal curve (dashed line) seems to give a much better fit rather than the Gaussian curve (chain line).

$$\sigma^2 = \begin{cases} \sigma_1^2 & \text{for } \ell_{\max} \le \ell_{B_f} \\ \dfrac{\sigma_1^2(\ell_{B_f}+1)^2 + \sigma_2^2\{(\ell_{\max}+1)^2 - (\ell_{B_f}+1)^2}{(\ell_{\max}+1)^2} & \text{for } \ell_{\max} > \ell_{B_f} \end{cases} \quad (3)$$

with $\ell_{B_f} = 60\ \hbar$ for the ($^{238}U + ^{12}C$) system [3]. When we assume $\sigma_1^2 = 560$ and $\sigma_2^2 = 762$ (amu)^2 so as to reproduce the FWHM = 65.0 amu at $E_{CM} = 228$ MeV, Eq. (3) gives the total width as illustrated with a solid line in Fig. 5.

Observed variances do not, however, follow Eq. (3) above the critical energy. Therefore, it is obvious that the width of fast fission can not be controlled by the stiffness coefficient and the temperature as discussed by Grègoire et al. [6] but it is rather provoked by the appearance of far-asymmetric mass distribution associated with the set-in of fast fission as concluded in Figs. 3 and 4. It follows that the mechanism of fast fission is different from any previously discussed.

References

[1] S. Cohen, F. Plasil, W.J. Swiatecki, Ann. Phys. (N.Y.). 82 (1974) 557.
[2] M.G. Mustafa, P.A. Baisden, H. Chandra, Phys. Rev. C25 (1982) 2524.
[3] A.J. Sierk, Phys. Rev. C33 (1986) 2039.
[4] H. Baba, A. Shinohara, T. Saito, N. Takahashi, A. Yokoyama, J. Phys. Soc. Jpn. 66 (1997) 998.
[5] C. Lebrun, F. Hanappe, J.F. Lecolley, F. Lefebvres, C. Ngô, J. Péter, B. Tamain, Nucl. Phys. A321 (1979) 207.
[6] C. Grégoire, R. Lucas, C. Ngô, B. Schürmann, H. Ngô, Nucl. Phys. A361 (1981) 443.
[7] B. Borderie, M. Berlanger, D. Gardes, F. Hanappe, L. Nowicki, J. Péter, B. Tamain, Z. Phys. A. 299 (1981) 263.
[8] C. Grégoire, C. Ngô, B. Remaud, Nucl. Phys. A383 (1982) 392.
[9] C. Grégoire, C. Ngô, E. Tomasi, B. Remaud, F. Scheuter, Nucl. Phys. A387 (1982) 37c.
[10] E.F. Hefter, Il Nuovo Cimento. 72A (1982) 1.
[11] C. Ngô, C. Grégoire, B. Remaud, E. Tomasi, Nucl. Phys. A400 (1983) 259c.
[12] Z. Zheng, B. Borderie, D. Gardes, H. Gauvin, F. Hanappe, J. Peter, M.F. Rivet, B. Tamain, A. Zaric, Nucl. Phys. A422 (1984) 447.
[13] S. Leray, X.S. Chen, G.Y. Fan, C. Grégoire, H. Ho, C. Mazur, C. Ngô, A. Pfoh, M. Ribrag, L. Schad, E. Tomasi, J.P. Wurm, Nucl. Phys. A423 (1984) 175.
[14] B. Heusch, H. Freiesleben, W.F.W. Schneider, B. Kohlmeyer, H. Stege, F. Pühlhofer, Z. Phys. A. 322 (1985) 309.
[15] A. Van Geertruyden, Ch. Leclercq–Willain, Nucl. Phys. A459 (1986) 173.
[16] A. Van Geertruyden, Ch. Leclercq–Willain, Nucl. Phys. A459 (1986) 196.
[17] P. Gippner, U. Brosa, H. Feldmeier, R. Schmidt, Phys. Lett. B. 252 (1990) 198.
[18] N. Takahashi, N. Yukawa, H. Kobayashi, A. Yokoyama, T. Saito, H. Baba, Z. Phys. A353 (1995) 35.
[19] M.–C. Duh, H. Baba, N. Takahashi, A. Yokoyama, T. Saito, S. Baba, K. Hata, Nucl. Phys. A550 (1992) 281.
[20] H. Baba, H. Okashita, S. Baba, T. Suzuki, H. Umezawa, H. Natsume, J. Nucl. Sci. Tech. (Tokyo). 8 (1971) 703.
[21] H. Baba, T. Sekine, S. Baba, H. Okashita, Japan Atomic Energy Research Institute report, JAERI 1227 (1972)
[22] N. Shirasu, H. Baba, to be published in Japan Atomic Energy Research Institute M-report.
[23] U. Reus, W. Westmeier, At. Data and Nucl. Data Tables 29, 1 (1983): evaluated nuclear structure data file of National Nuclear Data Center, BNL, U.S.A.
[24] C.H. Lee, Y.W. Yu, D. Lee, H. Kudo, K.J. Moody, G.T. Seaborg, Phys. Rev. C38 (1988) 1757.
[25] H. Umezawa, S. Baba, H. Baba, Nucl. Phys. A160 (1971) 65.
[26] A. Yokoyama, N. Takahashi, N. Nitani, H. Baba, R. Kasuga, T. Yamaguchi, D. Yano, K. Takamiya, N. Shinohara, K. Tsukada, Y. Hatsukawa, Y. Nagame, Z. Phys. A356 (1996) 55.
[27] H. Baba, A. Yokoyama, N. Takahashi, N. Nitani, R. Kasuga, T. Yamaguchi, D. Yano, K. Takamiya, N. Shinohara, K. Tsukada, Y. Hatsukawa, Y. Nagame, Z. Phys. A356 (1996) 61.